Article ID: 1000-324X(2013)03-0341-06 **DOI:** 10.3724/SP.J.1077.2012.12474

Preparation of Manganese Dioxide for Oxygen Reduction in Zinc Air Battery by Hydro thermal Method

HUANG You-Ju[1], LI Wei-Shan[1,2,3]

(1. School of Chemistry and Environment, South China Normal University, Guangzhou 510006, China; 2. Key Laboratory of Electrochemical Technology on Energy Storage and Power Generation of Guangdong Higher Education Institutes, South China Normal University, Guangzhou 510006, China; 3. Engineering Research Center of Materials and Technology for Electrochemical Energy Storage (Ministry of Education), South China Normal University, Guangzhou 510006, China)

Abstract: δ-MnO_2, α-MnO_2 and β-MnO_2 nano-particles were obtained by a hydrothermal method with changing molar ratios of K^+/H^+ at low temperature of 180℃, and the molar ratios of K^+/H^+ were 3.4, 0.85 and 0.24, respectively. The as-prepared samples were characterized by SEM, XRD, FTIR, BET, TG and electrochemical method. The results indicate that the concentrations of K^+ ion and H^+ ion have great effects on the crystalline structures, morphology and specific surface area of the as-prepared products. Among the three as-prepared samples used as cathodic materials in zinc air battery, the rate performances of the δ-MnO_2 and α-MnO_2 are superior to that of the as-prepared β-MnO_2. The oxygen reduction currents of δ-MnO_2, α-MnO_2, and β-MnO_2 at –0.35 V are 56.28, 56.01 and 40.88 mA/cm^2, respectively.

Key words: oxygen reduction; manganese dioxide; hydro thermal method; zinc air battery

In the development of metal-air batteries or fuel cells, the high performance electrocatalysts for air cathode is an important issue. Various types of electrocatalysts, *e.g.*, Pt and Pt-Ru alloys have been investigated as a key component of the electrodes, however, they are expensive. Significant progress has been made in recent years in the development of economical electrocatalysts, such as perovskite, spinels, pyrochlores, other oxides, pyrolyzed macrocycles, *etc*. Among the alternatives for platinum catalysts, MnO_2 is the best promising due to its low cost, its high catalytic activity for the oxygen reduction[1], protonelectron intercalation properties[2]. It is also well known as chemical oxidation catalysts and magnetic materials[3-4]. The performance of air electrode composed of $KMnO_4$ catalyst for oxygen reduction reaction has also been examined[5]. Some studies have been reported on its oxygen reduction characteristics[6]. Burchardt[7] has evaluated the electrocatalytic activity and stability for air electrodes.

MnO_2 has many polymorphic forms with different properties, such as α-, β-, γ- and δ-types. Several methods have been developed for the preparation of nanoscale manganese dioxides, including Sol-Gel templating[8], the thermal decomposition[9], refluxing[10], solvent-free solid reaction[11], electrodeposition[12], hydrothermal methods[13-27] and others[28]. Recent reports on the hydrothermal preparation of manganese dioxides has mainly involved redox reaction of MnO^{4-} and/or Mn^{2+} or the phase transformation of granular manganese dioxide precursors. De-Guzman, *et al*[13] prepared fibrous α-MnO_2 through the redox reaction between $KMnO_4$ and $MnSO_4$. The effects of pH and temperature on the crystalline structures of the final products were discussed. β-MnO_2 was obtained when the temperature was kept above 120℃. Wei, *et al*[19] synthesized α-MnO_2 and β-MnO_2 single-crystal nanowires by hydrothermal treatment of γ-MnO_2 at different temperatures. Shen, *et al*[20] reported the preparation of octahedral molecular sieve manganese oxide nanomaterials with different tunnel sizes by controlling the pH of the hydrothermal transformation of layered manganese dioxide precursors.

The synthesis and characterization of different crystalline MnO_2 have been the main subjects of many studies, but limited attention has been paid on the effect of different molar ratios of K^+/H^+ on the crystalline structures and electrochemical properties of the final MnO_2 products.

In this work, we report a hydrothermal method for synthesis of α-MnO_2, β-MnO_2 and δ-MnO_2 by using the same reaction with different molar ratios of K^+/H^+ at low temperature of 180℃. The morphology and electrochemical

Received date: 2012-08-07; **Modified date:** 2012-10-30; **Published online:** 2012-11-20
Foundation item: National Natural Science Foundation of China (20873046); Natural Science Foundation of Guangdong Province (10351063101000001)
Biography: HUANG You-Ju (1980–), female, candidate of PhD. E-mail: youjuhuang@163.com
Corresponding author: LI Wei-Shan, Professor. E-mail: liwsh@scnu.edu.cn

properties of the as-prepared MnO_2 were characterized. The results show that different molar ratios of K^+/H^+ can influence the crystalline structures and electrochemical properties of the final MnO_2 products.

1 Experimental

1.1 Preparation of MnO_2 electrocatalysts

All reagents were analytical grade and used as received without further purification. Distilled water was used in preparation and measurements. $KMnO_4$ (99.5%) and HNO_3 (65%–68%) were supplied by Guangzhou Haizhu Zone Chemical Reagent Company.

The samples were obtained in a typical synthesis using $KMnO_4$ and HNO_3 with a molar ratio of about 3.4:1(a1), 0.85:1(b1) and 0.2:1(c1), respectively. The weight of $KMnO_4$ for synthesizing sample a1, b1 and c1 is 0.79, 0.79 and 0.2 g, respectively, while the concentration of HNO_3 is 0.05, 0.2 and 0.2 mol/L (all for the volume of 30 mL). $KMnO_4$ was dissolved in HNO_3 under stirring for 30 min condition. The solution was transferred to a Teflon-lined stainless-steel autoclave, sealed and maintained at 180℃ for 24 h. The brown-black precipitates were filtered and washed with distilled water for several times to remove the unreacted materials and excess materials. The washing was done until the pH value of the washed water was 7. The resulting products were finally dried at 80℃ for 24 h in air.

1.2 Preparation of air electrodes

Air electrodes for performance evaluation were produced in two layers: the catalyst layer on the electrolyte side and a waterproof diffusion layer on the gas side. The active layer was composed of a catalyst (typically 80wt%), Vulcan XC-72 (10wt%, Hexing Chemical Industry Co., Ltd) and PTFE (10wt%, Dupont). The as-prepared catalysts (a1, b1 and c1) were used as the active material in air electrode. A slurry of the above mixture was made using absolute alcohol as a solvent. Then it was sandwiched in two foamed nickel foils, subsequently compressed for 3 min at 5×10^3 kg/cm^2 under 120℃ to obtain the air electrode.

1.3 Physical characterization

The phase structure of the as-prepared MnO_2 samples was recorded by X-ray diffraction (Rigaku D/max 2200 vpc). And the morphologies of samples were examined with scanning electron microscope (SEM, JEOL JSM-6490LV). Thermal properties were measured on a thermogravimetric analyzer (NETZSCH 409PC, Germany) with a heating rate of 10 K/min from 50℃ to 280℃. In the test process, nitrogen was used as the purge gas at a flow rate of 50 mL/min. The Brunauer-Emmett-Teller (BET) specific surface area was determined with a specific surface area instrument (ASAP2020M, Japan). The IR spectra were recorded on a Fourier transformation infrared (FTIR) spectrometer (IR Prestige-20, Shimadzu, Japan).

1.4 Electrochemical measurements

Linear sweep voltammetry were performed in a three-electrode configuration on an electrochemical station (CHI 650, Wuhan, China). 6 mol/L KOH solution was used as the electrolyte. The prepared air electrodes were used as the working electrode with the working area of 2 cm × 2 cm. A homemade Hg/HgO electrode was used as reference electrode. In the linear sweep voltammetry, a platinum sheet was used as the counter electrode and the scan rate was 1 mV/s. In the battery performance determination, a zinc sheet was used as the anode. To prevent moisture penetrating from the outside and flooding-out of the electrolyte from the inside of the cell, a PTFE sheet was attached to the cathode side that was open to the air.

The discharge tests of the simulated cells were performed on CT2001A (WUHAN, CHINA) and were discharged to an end voltage of 0.9 V at different constant currents of 1, 5 and 10 mA/cm^2.

All measurements were carried out at 25℃ (with an accuracy of 0.05℃) using a water thermostat. To make the results reproducible and reliable, a fresh electrolyte solution was used in every measurement.

2 Results and discussion

2.1 XRD analysis

Figure 1 shows the XRD patterns of the as-prepared products. From Fig. 1, it is obvious that the sample a1, b1 and c1 belong to δ-MnO_2, α-MnO_2 and β-MnO_2, respectively. The ratio of K^+ ion to H^+ ion exerts a decisive influence on the crystal structure of the products. When H^+ ion concentration is lower than that of K^+ ion (n_{k+}/n_{H+}=3.4), the observed product is δ-MnO_2 as de-

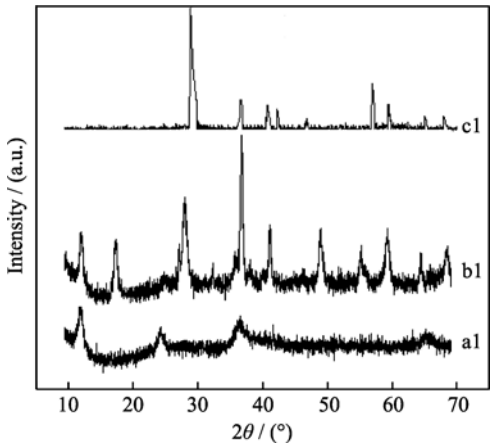

Fig. 1 XRD patterns for three types of the as-prepared samples a1:δ-MnO_2; b1:α-MnO_2; c1:β-MnO_2

scribed above, which is layered crystal structure. When H^+ ion concentration is about equal to that of K^+ ion (n_{k+}/n_{H+}=0.85), the product is converted to α-MnO_2. Under the condition of lower concentration of K^+ ion and higher concentration of H^+ ion (n_{k+}/n_{H+}=0.24), the obtained product is β-MnO_2. The result indicates that K^+ ion can serve as a template for the formation of the [2×2] tunnel structure of α-MnO_2 while H^+ ion cannot be the template for it. The formation of β-MnO_2 is no need for template ion, and the tendency to form β-MnO_2 at low K^+ concentration is rationalized. Main reasons are as follow: the polymorphs of α- and δ-type are different from β-type that the α- and δ-type are constructed from double chains of [MnO_6] octahedral forming [2×2] tunnels, while the β-type is composed of single chain of octahedral forming [1×1] tunnels, and β-MnO_2 is the thermodynamically stable phase and other MnO_2 phases tend to be converted to β-MnO_2 under appropriate condition[29].

Therefore, K^+ served as template for the formation of double chains of [MnO_6] octahedral forming [2×2] tunnels. It can be noted that sample c1 shows better crystalline than samples a1 and b1. This phenomenon can be ascribed to the different H^+ concentration. The higher H^+ concentration reduces the formation rate of manganese dioxide and thus favors the formation of better crystalline of the product (c1).

2.2 FTIR analysis

FT-IR spectra of the as-prepared MnO_2 samples are shown in Fig. 2. The bands at around 3420, 2366, 1622 and 1136 cm^{-1} correspond to the O–H vibrating mode of absorbed water. The band located at about 580 cm^{-1} on curve a1 in Fig. 2(B) is attributed to the metal-oxygen (Mn–O) bending vibration in δ-MnO_2. The bands located at 590 and 510 cm^{-1} belong to the metal-oxygen (Mn–O) bending vibration of [MnO_6] octahedral in α-MnO_2 as shown in Fig.2(B) (b1)[30], while the bands located at 714, 523 and 469 cm^{-1} correspond to the metal-oxygen (Mn–O) bending vibration of β-MnO_2 as shown in Fig. 2(B)(c1)[31]. The result of FT-IR spectra is consistent with the XRD result.

2.3 TG analysis

The results of TG analysis of the as-prepared samples are shown in Fig. 3. From the TG profiles, it can be seen that the samples show different thermal behavior. Two major weight losses occur between 50℃ and 280℃. The first weight loss (1.65wt%, 1.73wt% and 1.62wt% for a1, b1 and c1, respectively) below 120℃ can be attributed to desorption of physisorbed water whilst the release of chemisorbed water may be responsible for the significant weight loss (6.43wt%, 6.08wt% and 4.95wt% for a1, b1 and c1, respectively) occurred between 120 and 280℃.

2.4 SEM analysis and BET specific surface area

The morphology of the as-prepared samples was observed by SEM, as shown in Fig. 4. From Fig. 4(a), it can be seen that the product particles are uniformly distributed and the products are mainly composed of spherical-like particles with 250 nm of average grain size. For the active material, the smaller particles have larger specific surface area and shorter diffusion distance, which provides better rate performance. Fig. 4(b) shows the existence of the opening hydrangea like morphologies and the nanostructued particles in the as-prepared b1 sample (about 500 nm). Figure 4(c) shows that there exists a great deal of large particles of MnO_2, which consisted of aggregation of

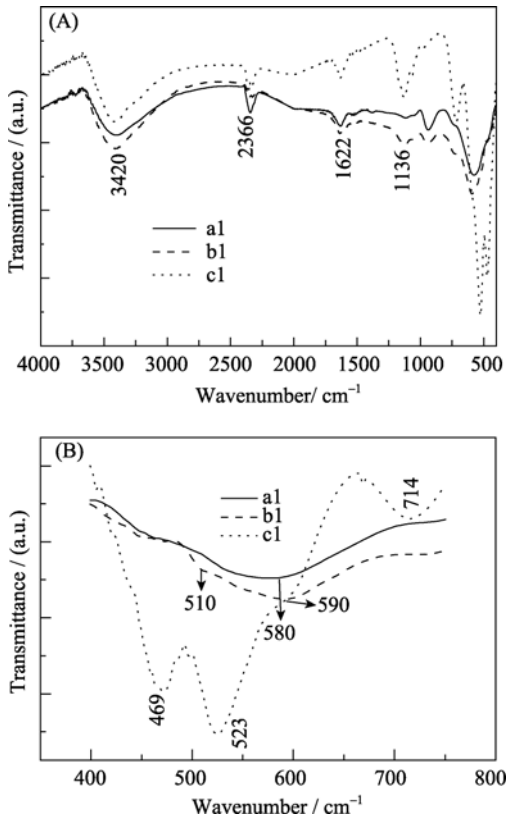

Fig. 2　FT-IR spectra of the as-prepared samples
a1: δ-MnO_2; b1:α-MnO_2; c1:β-MnO_2

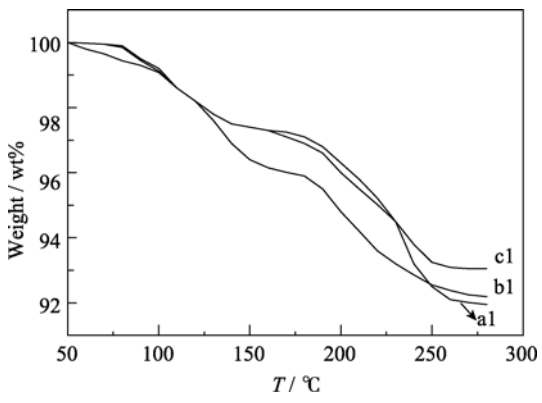

Fig. 3　TG analysis for the as-prepared samples
a1:δ-MnO_2; b1:α-MnO_2; c1:β-MnO_2

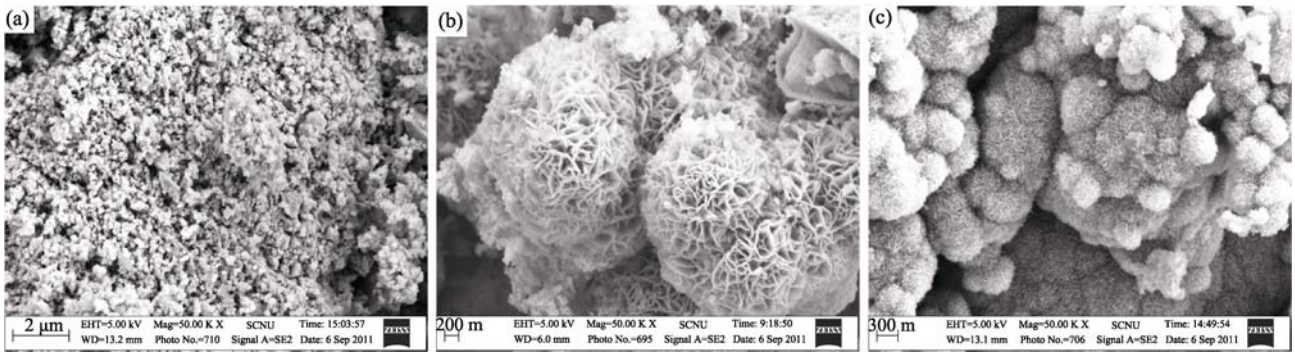

Fig. 4 SEM images of the as-prepared samples
(a) a1(δ-MnO_2); (b) b1(α-MnO_2); (c) c1(β-MnO_2)

MnO_2 hystrichosphere particles (about 250 nm). Thus, the morphology can be affected by the concentrations of the reactants. However, the actual mechanism is not clear for the moment and needs to be further investigated.

The BET surface areas of the samples, as shown in Table 1, are 68.2, 67.8 and 62.1 m^2/g for a1 (δ-MnO_2), b1 (α-MnO_2) and c1 (β-MnO_2), respectively. Compared to c1, the specific surface areas of a1 and b1 are increased by 9.8% and 9.2%, respectively.

2.5 Polarization curves for the ORR on the catalysts

Steady state polarization curves for the as-prepared samples are presented in Fig. 5. The current density was obtained based on the area of the work electrode because the electrodes contained the as-prepared catalysts with the same weight. As seen in Fig. 5, the initial oxygen reduction potentials for the electrodes consisting of the as-prepared catalysts are –0.04 V (c1), –0.05 V (a1) and –0.05 V (b1). Subsequently, with scanning potential becoming more negative, the reduction current increases slowly. The oxygen reduction current of the as-prepared samples (a1, b1 and c1) at –0.35 V is 56.28, 56.01 and 40.88 mA/cm^2, respectively. Compared with b1 (α-MnO_2) and c1 (β-MnO_2), the catalytic oxygen reduction current of a1 (δ-MnO_2) is increased by 0.48% and 37.67%, respectively. The results suggest that the catalytic activity of the as-prepared catalysts is related to not only the specific surface area but also the crystal structure. The activity towards oxygen reduction of the as-prepared samples is in the order: δ-MnO_2 ≈α-MnO_2 >β-MnO_2, which is in agreement with the other reports[32].

2.6 Electrochemical testing of the experimental cell

Figure 6 shows the discharge curves of the as-prepared samples a1 (δ-MnO_2), b1 (α-MnO_2) and c1(β-MnO_2) as cathodes in 6 mol/L KOH. From Fig. 6, it is clear that all the three electrodes exhibit smooth discharge curves. At a current rate of 1 mA/cm^2, a1, b1 and c1 have an open-circuit voltage of 1.38, 1.35 and 1.35 V, and a discharge plateau at 1.22, 1.22 and 1.20 V, respectively. The discharge capacity of a1, b1 and c1 is 231, 229 and 220 mA·h, respectively, as shown in the curves a, d and h. In addition, at a high rate of 5 mA/cm^2, the open-circuit

Table 1 Specific surface area of as-prepared samples

As-prepared sample	Specific surface area/($m^2 \cdot g^{-1}$)
a1(δ-MnO_2)	68.2
b1(α-MnO_2)	67.8
c1(β-MnO_2)	62.1

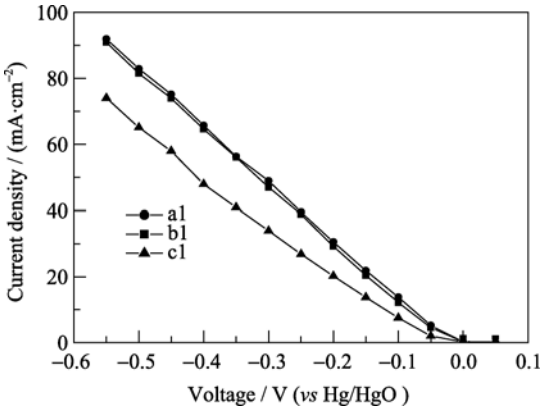

Fig. 5 Cathodic polarization curves for oxygen reduction on gas diffusion electrodes in 6 mol/L KOH solution
a1: (δ-MnO_2); b1: (α-MnO_2); c1: (β-MnO_2). Scan rate: 1 mV/s

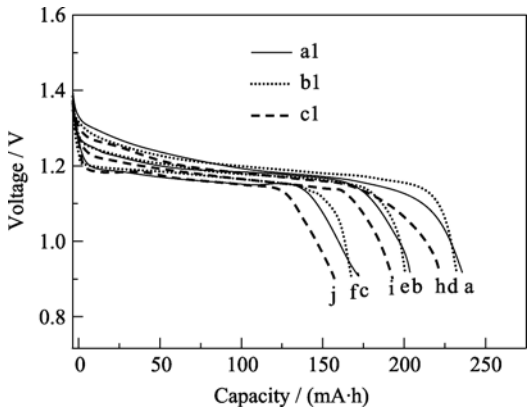

Fig. 6 Discharge curves of air/Zn batteries using as-prepared δ-MnO_2 (a, b and c), α-MnO_2 (d, e and f) and β-MnO_2 (h, I and j) at 1, 5 and 10 mA/cm^2, respectively

voltage of a1, b1 and c1 is 1.20, 1.20 and 1.18 V, respectively. And the discharge capacity of the catalysts is 205 mA·h (a1), 203 mA·h (b1) and 186 mA·h (c1). When the current rates was increased to 10 mA/cm^2, the discharge capacity of a1, b1 and c1 were decreased to 175, 174 and 160 mA·h, respectively. With increasing current rate, the reduction of the discharge capacity of a1 is equal to that of b1, but smaller than that of the c1. This phenomenon can be ascribed to the better crystalline, which does not favor the conduction of proton and electron during oxygen reduction reaction.

3 Conclusion

The effect of the concentration of K^+ ion and H^+ ion on the microcrystals type and the surface morphology of the products synthesized by a hydrothermal method, and the relationship between the microcrystals type and electrochemical performance were investigated in the paper. XRD and SEM images show that the as-prepared samples are δ-MnO_2 (a1), α-MnO_2 (b1) and β-MnO_2 (c1), obtained by a hydrothermal method with different concentration ratio of C_{k}^{+}/C_{H}^{+}=3.4, C_{k}^{+}/C_{H}^{+}=0.85 and C_{k}^{+}/C_{H}^{+}=0.2, respectively, indicating that δ-MnO_2 nanorods can be synthesized by controlling the concentration ratio of K^+/H^+ in the solution. The all three as-prepared MnO_2 samples contain physisorbed water and chemisorbed water which doesn't affect the catalystic activity of the samples. The sequence of the as-prepared samples is δ-MnO_2≈α-MnO_2> β-MnO_2 in the catalystic oxygen reduction activity, which is in agreement with the sequence of the surface area of the samples. It is obvious that the concentration of K^+ ion and H^+ ion has a strong effect on the structure, morphology and electrochemical properties of the different type MnO_2 products.

References:

[1] Mao L Q, Zhang D, Sotomura T, *et al*. Mechanistic study of the reduction of oxygen in air electrode with manganese oxides as electrocatalysts. *Electrochim Acta*, 2003, **48(8):**1015–1021.

[2] Rebello J S, Samant P V, Figueiredo J L, *et al*. Enhanced electrocatalytic activity of carbon-supported MnO_x/Ru catalysts for methanol oxidation in fuel cells. *J. Power Sources*, 2006, **153(1):** 36–40.

[3] Nurmaimaiti, Xia X. Synthesis and performance of nano phase α-MnO_2. *Journal of Inorganic Materials*, 2000, **15(5):** 802–806.

[4] Zhu L C, Yuan Z Z, Li W S. Influence of composition on the electrochemical performance of EMD. *Journal of Inorganic Materials*, 2005, **20(2):** 489–493.

[5] Yang C C. Preparation and characterization of electrochemical properties of air cathode electrode. *Int. J. Hydrogen Energy*, 2004, **29(2):** 135–143.

[6] Verma A, Jha A K, Basu S. Manganese dioxide as a cathode catalyst for a direct alcohol or sodium borohydride fuel cell with a flowing alkaline electrolyte. *J. Power Sources*, 2005, **141(1):** 30–34.

[7] Burchardt T. An evaluation of electrocatalytic activity and stability for air electrodes. *J. Power Sources*, 2004, **135(1/2):** 192–197.

[8] Lakshmi B L, Patrissi C J, Martin C R. Sol-Gel template synthesis of semiconductor oxide micro- and nanostructures. *Chem. Mater.*, 1997, **9(11):** 2544–2550.

[9] Zitoun D, Pinna N, Frolet N, *et al*. Single crystal manganese oxide multipods by oriented attachment. *J. Am. Chem. Soc.*, 2005, **127(43):** 15034–15035.

[10] Villegas J C, Garces L J, Gomez S, *et al*. Particle size control of cryptomelane nanomaterials by use of H_2O_2 in acidic condition. *Chem. Mater.*, 2005, **17(11):**1910–1918.

[11] Ding Y S, Shen X F, Sithambaram S, *et al*. Synthesis and catalytic activity of cryptomelane-type manganese dioxide nanomaterials produced by a novel solvent-free method. *Chem. Mater.*, 2005, **17(21):** 5382–5389.

[12] Wu M S, Lee J T, Wang Y Y, *et al*. Field emission from manganese oxide nanotubes synthesized by cyclic voltammetric electrodeposition. *J. Phys. Chem. B*, 2004, **108(42):** 16331-16333.

[13] DeGuzman R N, Shen Y F, Neth E J, *et al*. Synthesis and characterization of octahedral molecular sieves (OMS-2) having the hollandite structure. *Chem. Mater.*, 1994, **6(6):** 815–821.

[14] Wang X, Li Y D. Synthesis and formation mechanism of manganese dioxide nanowires/nanorods. *Chem. Eur. J.*, 2003, **9(1):** 300–306.

[15] Zhou F, Zheng H G, Zhao X M, *et al*. Large-area synthesis of high-quality β-MnO_2 nanowires and the mechanism of formation through a facile mineralization process. *Nanotechnology*, 2005, **16:** 2072–2076.

[16] Yuan J K, Li W N, Gomez S, *et al*. Shape-controlled synthesis of manganese oxide octahedral molecular sieve three-dimensional nanostructures. *J. Am. Chem. Soc.*, 2005, **127(41):**14184–14185.

[17] Zheng D S, Sun S X, Fan W L, *et al*. One-step preparation of single-crystalline β-MnO_2 nanotubes. *J. Phys. Chem. B*, 2005, **109(34):** 16439–16443.

[18] Wu C Z, Xie Y, Wang D, *et al*. Selected-control hydrothermal synthesis of γ-MnO_2 3D nanostructures. *J. Phys. Chem. B*, 2003, **107(49):** 13583–13587.

[19] Wei M D, Konishi Y, Zhou H S, *et al*. Synthesis of single-crystal manganese dioxide nanowires by a soft chemical process. *Nanotechnology*, 2005, **16(2):** 245–249.

[20] Shen X F, Ding Y S, Liu J, *et al*. Control of nanometer-scale tunnel sizes of porous manganese oxide octahedral molecular sieve nanomaterials. *Adv. Mater.*, 2005, **17(7):** 805–809.

[21] Cheng F Y, Zhao J Z, Song W N, *et al*. Facile controlled synthesis of MnO_2 nanostructures of novel shapes and their application in batteries. *Inorg. Chem.*, 2006, **45(5):** 2038–2044.

[22] Tang B, Wang G L, Zhuo L H, *et al*. Novel dandelio-like beta-manganese dioxide microstructures and their magnetic properties. *Nanotechnology*, 2006, **17(4):** 947–951.

[23] Cheng F Y, Chen J, Gou X L, *et al*. High-power alkaline Zn-MnO_2 batteries using γ-MnO_2 nanowires/nanotubes and electrolytic zinc powder. *Adv. Mater.*, 2005, **17(22):** 2753–2756.

[24] Ding Y S, Shen X F, Gomez S, *et al*. Hydrothermal growth of manganese dioxide into three-dimensional hierarchical nanoarchitectures. *Adv. Funct. Mater.*, 2006, **16:** 549–555.

[25] Li W N, Yuan J K, Gomez-Mower S, *et al*. Synthesis of single crystal manganese oxide octahedral molecular sieve (OMS) nanostructures with tunable tunnels and shapes. *J. Phys. Chem. B*, 2006, **110(7):** 3066–3070.

[26] Li W N, Yuan J K, Shen X F, *et al*. Hydrothermal synthesis of structure- and shape-controlled manganese oxide octahedral molecular sieve nanomaterials. *Adv. Funct. Mater.*, 2006, **16:** 1247–1253.

[27] Wang H, Lu Z, Qian D, *et al*. Single-crystal α-MnO_2 nanorods: synthesis and electrochemical properties. *Nanotechnology*, 2007, **18(11):** 115616–115621.

[28] Huang Y J, LIN Y L, LI W S. Manganese Dioxide with high specific surface area for alkaline battery. *Chem. Res. Chinese Universities.* 2012, **28(5):** 874–877.

[29] Feng Q, Kanoh H, Ooi K. Manganese oxide porous crystals. *J. Mater. Chem.*, 1999, **9:** 319–333.

[30] Wang H E, Qian D. Synthesis and electrochemical properties of α-MnO_2 microspheres. *Mater. Chem. Phys.*, 2008, **109(2/3):** 399–403.

[31] Zhang L X, Liu C S, Zhuang L, *et al*. Manganese dioxide as an alternative cathodic catalyst to platinum in microbial fuel cells. *Biosens. Bioelectron.*, 2009, **24(9):** 2825–2829.

[32] Cao Y L, Yang H X, Ai X P, *et al*. The mechanism of oxygen reduction on MnO_2-catalyzed air cathode in alkaline solution. *J. Electroanal. Chem.*, 2003, **557:**127–134.

水热法合成锌空气电池氧还原二氧化锰催化剂

黄幼菊[1], 李伟善[1,2,3]

(华南师范大学 1. 化学和环境学院; 2. 广东高校电化学储能与发电技术重点实验室; 3. 教育部电化学储能材料与技术工程研究中心, 广州 510006)

摘 要: 在 180℃下通过改变 K^+与 H^+摩尔比使用水热法分别制备了 δ-MnO_2, α-MnO_2 和 β-MnO_2 纳米颗粒, K^+与 H^+摩尔比分别为 3.4、0.85 和 0.24。所合成的样品通过扫描电子显微镜(SEM), 粉末 X 射线衍射(XRD), 傅里叶变换红外光谱(FTIR), BET 比表面分析, 热重分析(TG)和电化学方法表征。结果表明: K^+与 H^+的浓度对产品的晶型、形貌以及比表面积有很大影响; 将这三种材料作为锌空电池的阴极材料时, δ-MnO_2与 α-MnO_2的电化学性能明显优于 β-MnO_2. 在 –0.35 V 下, δ-MnO_2、α-MnO_2 和 β-MnO_2 的氧还原电流分别为 56.28、56.01 和 40.88 mA/cm^2。

关 键 词: 氧还原; 二氧化锰; 水热方法; 锌空电池

中图分类号: TM9 **文献标识码:** A